ACS APPLIED MATERIALS & INTERFACES

Research Article

www.acsami.org

Excellent Toluene Sensing Properties of SnO_2–Fe_2O_3 Interconnected Nanotubes

Hao Shan,[†] Changbai Liu,[‡] Li Liu,*[,†] Jinbao Zhang,[†] Haiying Li,[†] Zhen Liu,[†] Xiaobo Zhang,[†] Xiaoqing Bo,[†] and Xiao Chi[†]

[†]State Key Laboratory of Superhard Materials, College of Physics, Jilin University, Changchun 130012, People's Republic of China

[‡]College of Electronic Science & Engineering, Jilin University, Changchun 130012, People's Republic of China

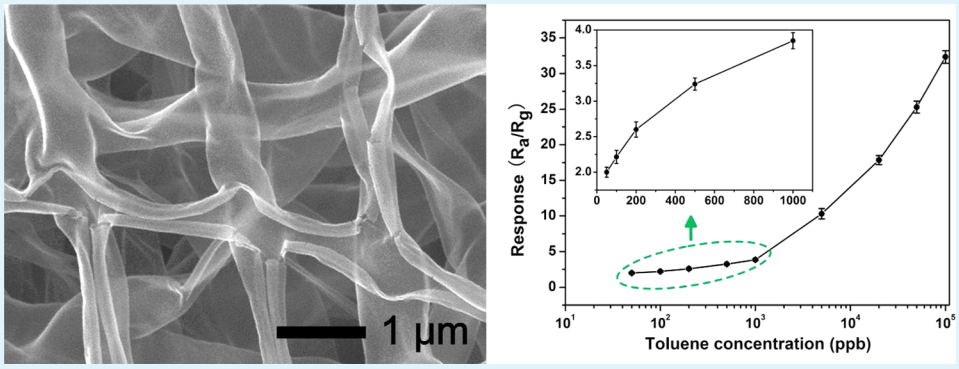

ABSTRACT: SnO_2–Fe_2O_3 interconnected nanotubes were obtained by combining the single nozzle electrospinning and thermal treatment methods. The results of scanning electron microscopy revealed the special structure of ruptures and interconnected nanotubes in the as-prepared materials. The toluene sensing test results of SnO_2–Fe_2O_3 interconnected nanotubes show that SnO_2–Fe_2O_3 interconnected nanotubes possess excellent toluene gas-sensing properties. The sensitivity of detecting limit (50 ppb) is 2.0 at the optimum operating temperature of 260 °C. The response and recovery times to 1 ppm toluene are about 5 and 11 s, respectively. Moreover, the SnO_2–Fe_2O_3 interconnected nanotube gas sensors exhibit the remarkable selectivity to toluene, and good long-term stability.

KEYWORDS: *SnO_2, Fe_2O_3, nanotubes, toluene, gas sensors, electrospinning*

1. INTRODUCTION

Semiconductor oxides have attracted a lot of attention around the world, due to their wide applications in luminescence,[1] photosensitization,[2,3] magnetism,[4,5] lithium batteries,[6,7] and gas sensors,[8,9] especially in the field of gas sensors, although numerous efforts have been done to improve the gas-sensing performance of a single semiconductor, their properties are still limited by some shortcomings, such as high operating temperature, low sensitivity, poor selectivity, and stability. Nowadays, a good deal of endeavors have been undertaken to solve these problems, aiming to enhance the gas-sensing properties of semiconductor oxides. One solution is to synthesize the composite semiconductor oxide materials. For instance, Wang et al. demonstrated that a SnO_2–CuO composite film possessed a higher sensitivity to H_2S.[10] Zhang et al. confirmed that ZnO-In_2O_3 nanofibers exhibited improved and excellent sensing properties to ethanol.[11] Chen et al. discovered that MoO_3–TiO_2 nanorods showed enhanced sensing properties to ethanol. However, the composite semiconductor oxide materials of Fe_2O_3 have rarely been reported.[12]

Fe_2O_3, an n-type semiconductor, which is one of the stable semiconductor oxides under ambient conditions, has been widely fabricated as gas sensors because of its good stability, lower cost, and easy availability. In this paper, we obtained SnO_2–Fe_2O_3 interconnected nanotubes (SFINs) by combining the single nozzle electrospinning and thermal treatment methods. Furthermore, the gas sensing properties of SFINs to toluene are also investigated. The results show that nanotubes display an excellent toluene sensing characteristic.

2. MATERIALS AND METHODS

2.1. Materials. Poly(vinyl pyrrolidone) (PVP, M_w = 1 300 000) was purchased from Sigma-Aldrich (USA). $Fe(NO_3)_3{\cdot}9H_2O$, $SnCl_2{\cdot}2H_2O$, *N*,*N*-dimethylformamide (DMF), and ethanol were obtained from Aladdin (China). The above chemical reagents used were analytical grade and used without further purification.

2.2. Synthesis of SnO_2–Fe_2O_3 Interconnected Nanotubes. The electrospinning procedure was according to the reported paper.[13] In a typical process, 0.4 g of $Fe(NO_3)_3{\cdot}9H_2O$ was mixed with 2.2 g of ethanol, and 0.021 g of $SnCl_2{\cdot}2H_2O$ was mixed with 2.2 g DMF. The two mixtures were under magnetic stirring at room temperature for 2 h. Subsequently, 0.4 g of PVP was added in after mingling these two

Received: April 24, 2013
Accepted: June 11, 2013
Published: June 11, 2013

 © 2013 American Chemical Society dx.doi.org/10.1021/am4015082 | *ACS Appl. Mater. Interfaces* 2013, 5, 6376–6380

mixed solutions, and kept stirring for 12 h. The mixture was then ejected from a glass syringe with a voltage of 15 kV. The distance between the cathode and anode was 30 cm. The as-electrospun composite nanofibers were calcinated at 600 °C for 4 h at the rate of 5 °C/min. Finally, the SFINs were obtained.

2.3. Characterization. Structure analysis with X-ray diffraction (XRD) was conducted on a PANalytical B.V. Empyrean X-ray diffractometer with Cu Kα radiation (λ = 1.5418 Å). Scanning electron microscope (SEM) images were performed on an FEI XL30 instrument equipped with an energy-dispersive spectrometer (EDS). Transmission electron micrograph (TEM) images were performed on a JEOL-2000EX. X-ray photoelectron spectroscopy (XPS) measurements were carried out on an ESCLAB KMII using Al as the exciting source.

2.4. Sensor Fabrication and Sensing Measurements. The processes of gas sensor fabrication and gas-sensing tests have been described in our previous work.[14] In this paper, the sensor sensitivity is defined as $\beta = R_a/R_g$, where R_a and R_g are the electrical resistance of the sensor in air and in the target gas, respectively. The time taken to achieve 90% of the resistance variation is defined as the response time. After taking the sensor out of the target gas, the time that the resistance returns 90% of the resistance variation is defined as the recovery time.

3. RESULTS AND DISCUSSION

3.1. Structural and Morphological Characteristics. The morphologies of SFINs are characterized by SEM and TEM. As shown in Figure 1a,b, all specimens display the structure of nanotubes and a bended morphology with the average diameters of about 500 nm. These nanotubes are connected with each other. Moreover, there are ruptures in the surface of nanotubes, which provide easy pathways for gas molecules to penetrate easily into the whole nanotubes. Figure 1c shows the TEM image of SnO_2–Fe_2O_3, which can confirm their structure of nanotubes (see the bright center and dark outer surface in the picture). The result is consistent with the SEM images above.

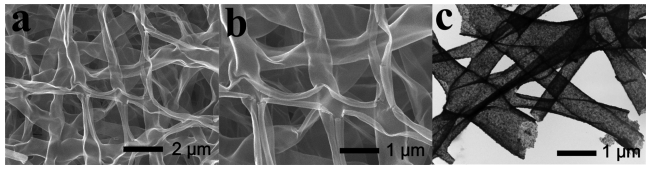

Figure 1. (a, b) SEM and (c) TEM images of SnO_2–Fe_2O_3 interconnected nanotubes.

The XRD pattern obtained from SFINs is shown in Figure 2a. All the peaks in the XRD pattern can be well indexed to hematite (JCPDS: 89-0597), indicating the formation of the rhombohedral Fe_2O_3. No peaks in the spectrum come from SnO_2, may be due to the small amount of $SnCl_2{\cdot}2H_2O$ in the precursor solution of electrospinning. Figure 2b shows the EDS pattern of SFINs, which indicates that the as-prepared materials are composed of O, Fe, and Sn elements. The further evidence for the existence of Sn can be examined by XPS, and the results are shown in Figure 3. Figure 3a shows the spectrum of Fe 2p, in which two peaks at 711.8 and 725.6 eV correspond to Fe $2p_{3/2}$ and Fe $2p_{1/2}$, respectively.[15] Furthermore, Figure 3b indicates that the binding energy of Sn $3d_{5/2}$ and Sn $3d_{3/2}$ are found at 486.6 and 495.1 eV, respectively. These are consistent with the reported values observed for SnO_2.[16]

3.2. Gas-Sensing Properties of SnO_2–Fe_2O_3 Interconnected Nanotubes. Gas-sensing tests are performed at different operating temperatures in order to find the optimum operating temperature. The relationship between the different operating temperatures and the response of the sensors to 50 ppm toluene is shown in Figure 4. From the figure, we can see that the response reaches the maximum value of 25.3 at 260 °C. This phenomenon can be explained by the balance between the speed of chemical reaction and the speed of gas diffusion. At low temperatures, the sensitivity gradually rises with the increasing of reaction temperature. However, the diffusion speed of the target gas is accelerated at high temperature. Thus, the two processes will tend to balance at a certain temperature, at which temperature the sensitivity of gas sensors attains the maximum.[17,18] Hence, 260 °C is the optimum operating temperature for SFIN gas sensors and is used in the following gas sensitive performance tests.

The comparison between SFIN gas sensors and some other toluene gas sensors can be seen in Table 1. It is clear to see that the sensors based on SFINs possess the higher sensitivity to toluene.

Figure 5 shows the sensitivities of SFIN gas sensors to different concentrations toluene in the range of 50 ppb to 100 ppm at 260 °C. The inset in Figure 5 shows the sensitivities of sensors at low toluene concentrations. It is clear to see that the SFIN gas sensors show an excellent sensitivity to toluene.

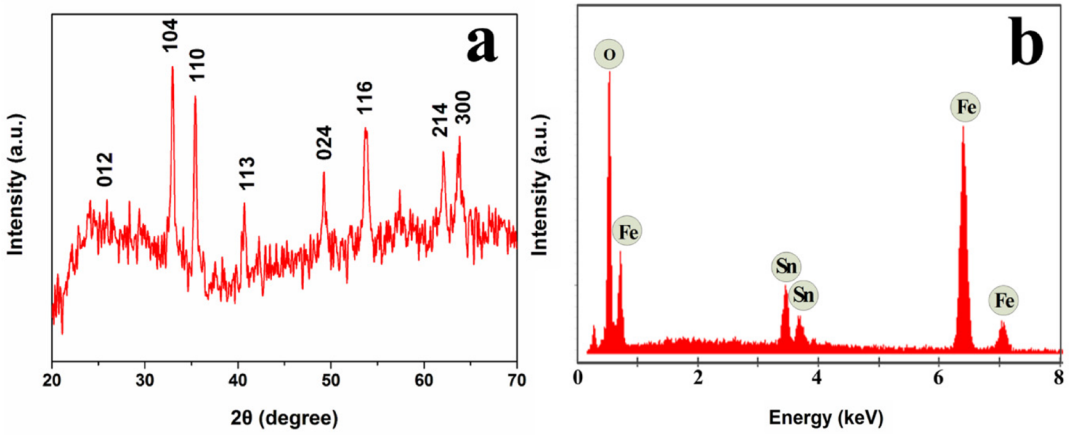

Figure 2. (a) XRD and (b) EDS patterns of SnO_2–Fe_2O_3 interconnected nanotubes.

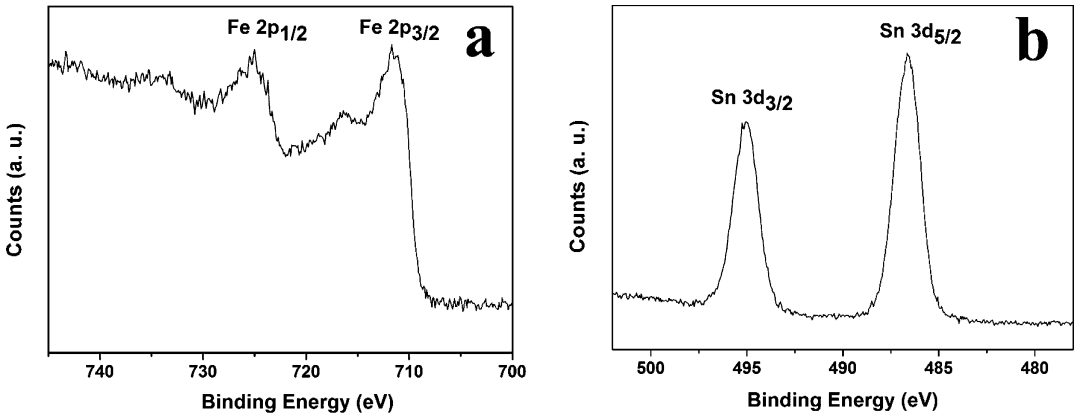

Figure 3. XPS spectra of (a) Fe 2p and (b) Sn 3d of the as-prepared SnO_2−Fe_2O_3 interconnected nanotubes.

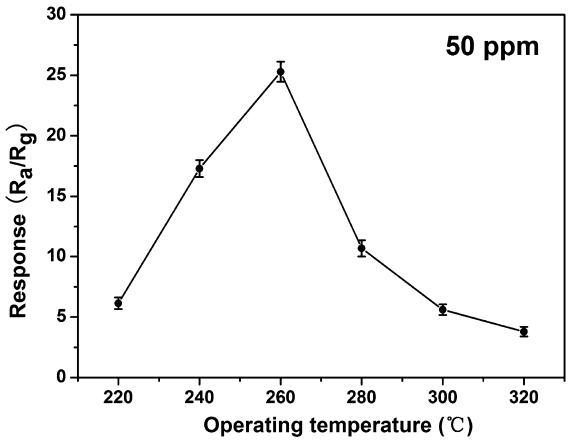

Figure 4. Sensitivities of SnO_2−Fe_2O_3 interconnected nanotube gas sensors to 50 ppm toluene at different operating temperatures.

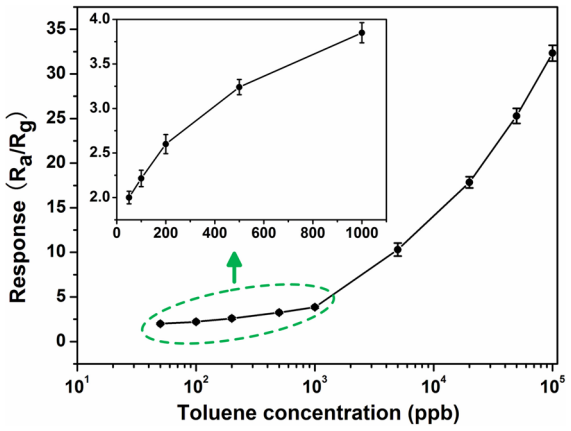

Figure 5. Sensitivities of SnO_2−Fe_2O_3 interconnected nanotube gas sensors to different concentrations of toluene in the range of 50 ppb to 100 ppm at 260 °C; the inset shows the sensitivities of sensors at low toluene concentrations.

When exposed to 50, 100, 200, and 500 ppb toluene, the sensitivities are 2.0, 2.2, 2.6, and 3.24, respectively.

The lowest detection limit of SFIN gas sensors to toluene is 50 ppb, which is much lower than that of P(VBC-*co*-MMA)-coated quartz crystal microbalance (QCM) sensors (54 ppm), P(HEMA-*co*-MA)-coated QCM sensors (72 ppm), poly(*β*-CD-*co*-MA)-coated QCM sensors (100 ppm), and polystyrene-coated quartz crystal nanobalance (QCN) sensors (3.5 ppm).[24−27] The lowest detecting limit of 50 ppb indicates that SFINs can be used as promising materials for fabricating high-performance toluene sensors.

To further investigate the gas-sensing properties of SFIN gas sensors, we present four response and recovery characteristic cycle curves of SFIN gas sensors to 1 ppm toluene, which are shown in Figure 6. No major changes in the response and recovery times are found from this figure, which can demonstrate the good repeatability characteristic of SFIN gas sensors. The average response and recovery times are about 5 and 11 s, respectively. Such short response and recovery times may be due to the special structure of SFINs. On one hand, the ruptures in nanotubes can offer more contact surface, which leads to more toluene molecules absorbed on the surface of the material. On the other hand, the interconnected nanotubes can be available for the transfer of oxygen molecules and toluene molecules to and from the reaction sites.

In our experiment, toluene, acetone, ethanol, formaldehyde, ammonia, hydrogen, carbon monoxide, and butane sensing characteristics of the SFIN gas sensors are also measured under the same conditions to estimate the selectivity of SFIN gas sensors. Figure 7 shows the sensitivities of SFIN gas sensors to 50 ppm of different gases at 260 °C. From the figure, we can see that SFIN gas sensors show less sensitivity to other gases, indicating the excellent selectivity to toluene.

Table 1. Comparison between SFIN Gas Sensors and Some Other Toluene Gas Sensors

gas sensor	toluene concentration (ppm)	definition of sensitivity	operating temperature (°C)	value of sensitivity (about)	ref
SnO_2−Fe_2O_3	50	R_a/R_g	260	25.3	this work
SnO_2	50	R_a/R_g	350	3	19
NiO-SnO_2	50	R_a/R_g	330	11	20
TiO_2−ZnO	50	R_a/R_g	290	10	21
SnO_2−ZnO	50	R_a/R_g	190	15.6	22
ZnO−SnO_2	50	R_a/R_g	360	6	23

dx.doi.org/10.1021/am4015082 | ACS Appl. Mater. Interfaces 2013, 5, 6376−6380

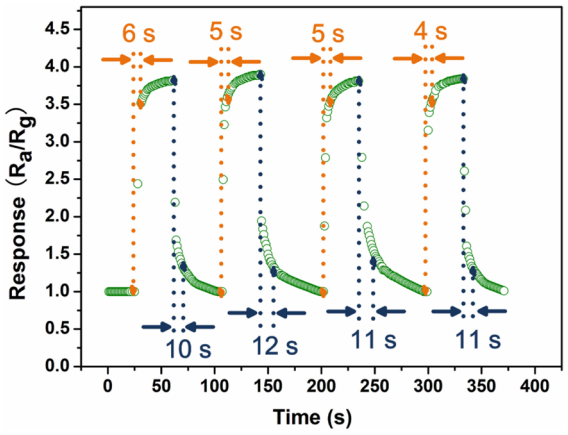

Figure 6. Response and recovery characteristic cycle curves of SnO_2–Fe_2O_3 interconnected nanotube gas sensors to 1 ppm toluene at 260 °C.

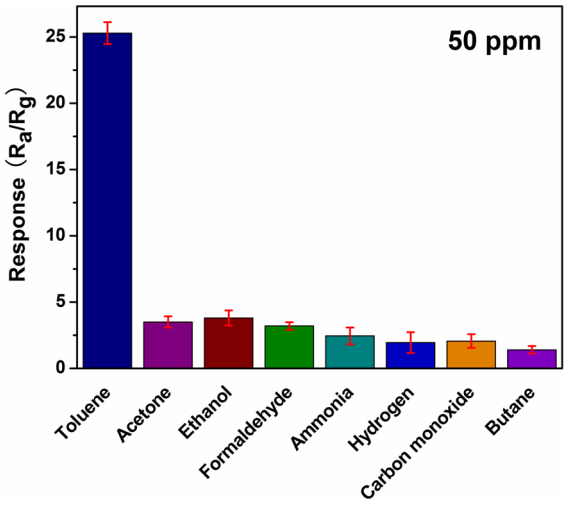

Figure 7. Sensitivities of SnO_2–Fe_2O_3 interconnected nanotube gas sensors to 50 ppm of different gases at 260 °C.

The long-term stability of SFIN gas sensors has been also measured and is shown in Figure 8. It can be seen that the sensors exhibit nearly constant sensor signals to 1, 5, 20, 50, and 100 ppm toluene during the test, confirming the good stability of the SFIN gas sensors.

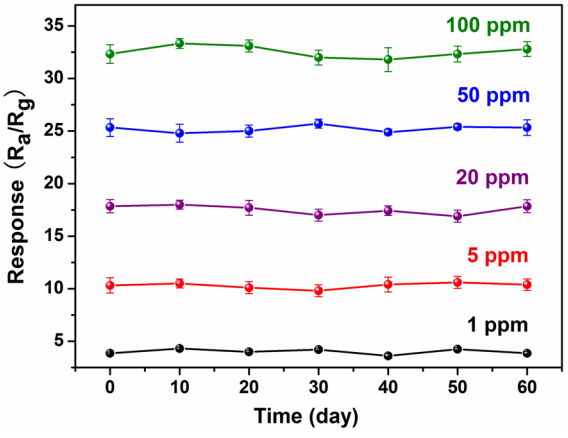

Figure 8. Long-term stability of SnO_2–Fe_2O_3 interconnected nanotube gas sensors to 1, 5, 20, 50, and 100 ppm toluene.

The sensing mechanism of semiconductor oxide gas sensors has been discussed in the previous literature.[19−21] In our experiment, it can be explained as follows. When Fe_2O_3 is in air, the surrounding oxygen molecules will capture free electrons from the surface of Fe_2O_3 and are ionized to O_2^-, O^-, and O^{2-}. Therefore, the depletion region is formed. The decreasing of carrier concentration and electron mobility results in the rise of resistance. On the contrary, in the toluene atmosphere, the reaction between ethanol molecules and oxygen species will release electrons. Thus, the resistance decreases.

In terms of the structure of materials, the ruptures of nanotubes can offer more contact and reaction sites, which will result in more toluene and oxygen absorbed on the surface of materials. Otherwise, the large surface of interconnected nanotubes makes the transfer of oxygen molecules and toluene molecules to and from the reaction sites more easy.

Compared with the other toluene gas sensors that have been reported, for instance, the gas sensors based on SnO_2 nanofibers,[19] the toluene sensing properties have been improved dramatically. This phenomenon can be ascribed to the heterojunctions that formed at the interfaces between SnO_2 and Fe_2O_3. These heterojunctions may result in an increase in the hole−electron separation efficiency between SnO_2 and Fe_2O_3.[28,29] Therefore, when SFINs meet toluene, more electrons transfer from the gas to the sensing material efficiently, and thus, the sensitivity of the sensor increases.

4. CONCLUSIONS

In summary, SnO_2–Fe_2O_3 interconnected nanotubes were synthesized by the single nozzle electrospinning method, and followed by thermal treatment methods. The toluene sensing properties were studied in our experiment. The results show that the optimum operating temperature to detect toluene is 260 °C. The lowest detecting limit to toluene is 50 ppb, and the response value is 2.0. The average response and recovery times to 1 ppm toluene are about 5 and 11 s, respectively. Otherwise, the four response and recovery characteristic cycle curves to 1 ppm toluene indicated the good repeatability characteristic of SnO_2–Fe_2O_3 interconnected nanotube gas sensors. Moreover, the sensors also exhibit excellent selectivity to toluene and good long-term stability.

AUTHOR INFORMATION

Corresponding Author

*E-mail: liul99@jlu.edu.cn. Tel: +86 431 8502260. Fax: +86 431 8502260.

Notes

The authors declare no competing financial interest.

ACKNOWLEDGMENTS

The work was supported by the Jilin Environment Office (2009-22), the Jilin Provincial Science and Technology Department (20100344), and the National Innovation Experiment Program for University Students (2010C65188).

REFERENCES

(1) Wu, X.; Siu, G.; Fu, C.; Ong, H. *Appl. Phys. Lett.* **2001**, *78*, 2285–2287.

(2) Kar, P.; Banerjee, T.; Verma, S.; Sen, A.; Das, A.; Ganguly, B.; Ghosh, H. N. *Phys. Chem. Chem. Phys.* **2012**, *14*, 8192–8198.

(3) Leschkies, K. S.; Divakar, R.; Basu, J.; Enache-Pommer, E.; Boercker, J. E.; Carter, C. B.; Kortshagen, U. R.; Norris, D. J.; Aydil, E. S. *Nano Lett.* **2007**, *7*, 1793−1798.
(4) Bhowmik, R. N.; Saravanan, A. *J. Appl. Phys.* **2010**, *107*, 053916.
(5) Fukumura, T.; Jin, Z.; Kawasaki, M.; Shono, T.; Hasegawa, T.; Koshihara, S.; Koinuma, H. *Appl. Phys. Lett.* **2001**, *78*, 958−960.
(6) Brandt, A.; Balducci, A. *J. Power Sources* **2013**, *230*, 44−49.
(7) Fehse, M.; Fischer, F.; Tessier, C.; Stievano, L.; Monconduit, L. *J. Power Sources* **2013**, *231*, 23−28.
(8) Gurlo, A. *Nanoscale* **2011**, *3*, 154−165.
(9) Zheng, W.; Li, Z.; Zhang, H.; Wang, W.; Wang, Y.; Wang, C. *Mater. Res. Bull.* **2009**, *44*, 1432−1436.
(10) Wang, X. D.; Wang, W.; Li, H. L.; Fu, C.; Ke, Y. B.; He, S. T. *Sens. Actuators, B* **2012**, *169*, 10−16.
(11) Zhang, X. J.; Qiao, G. J. *Appl. Surf. Sci.* **2012**, *258*, 6643−6647.
(12) Chen, Y. J.; Xiao, G.; Wang, T. S.; Zhang, F.; Ma, Y.; Gao, P.; Zhu, C. L.; Zhang, E. D.; Xu, Z.; Li, Q. H. *Sens. Actuators, B* **2011**, *155*, 270−277.
(13) Li, D.; Xia, Y. *Nano Lett.* **2003**, *3*, 555−560.
(14) Liu, L.; Liu, C.; Li, S.; Wang, L.; Shan, H.; Zhang, X.; Guan, H.; Liu, Z. *Sens. Actuators, B* **2013**, *177*, 893−897.
(15) Chen, Y. J.; Gao, X. M.; Di, X. P.; Ouyang, Q. Y.; Gao, P.; Qi, L. H.; Li, C. Y.; Zhu, C. L. *ACS Appl. Mater. Interfaces* **2013**, *5*, 3267−3274.
(16) Liu, L.; Li, S.; Wang, L.; Guo, C.; Dong, Q.; Li, W. *J. Am. Ceram. Soc.* **2011**, *94*, 771−775.
(17) Zhang, T.; Zeng, Y.; Fan, H. T.; Wang, L. J.; Wang, R.; Fu, W. Y.; Yang, H. B. *J. Phys. D: Appl. Phys.* **2009**, *42*, 045103.
(18) Lim, S. K.; Hwang, S. H.; Chang, D.; Kim, S. *Sens. Actuators, B* **2010**, *149*, 28−33.
(19) Qi, Q.; Zhang, T.; Liu, L.; Zheng, X. *Sens. Actuators, B* **2009**, *137*, 471−475.
(20) Liu, L.; Zhang, Y.; Wang, G.; Li, S.; Wang, L.; Han, Y.; Jiang, X.; Wei, A. *Sens. Actuators, B* **2011**, *160*, 448−454.
(21) Zeng, Y.; Zhang, T.; Wang, L.; Kang, M.; Fan, H.; Wang, R.; He, Y. *Sens. Actuators, B* **2009**, *140*, 73−78.
(22) Wei, S.; Zhang, Y.; Zhou, M. *Solid State Commun.* **2011**, *151*, 895−899.
(23) Song, X.; Zhang, D.; Fan, M. *Appl. Surf. Sci.* **2009**, *255*, 7343−7347.
(24) Fan, X.; Du, B. *Sens. Actuators, B* **2012**, *166−167*, 753−760.
(25) Fan, X.; Du, B. *Sens. Actuators, B* **2011**, *160*, 724−729.
(26) Ju, J. F.; Syu, M. J.; Teng, H. S.; Chou, S. K.; Chang, Y. S. *Sens. Actuators, B* **2008**, *132*, 319−326.
(27) Mirmohseni, A.; Abdollahi, H.; Rostamizadeh, K. *Sens. Actuators, B* **2007**, *121*, 365−371.
(28) Kang, J.; Kuang, Q.; Xie, Z. X.; Zheng, L. S. *J. Phys. Chem. C* **2011**, *115*, 7874−7879.
(29) Niu, M.; Huang, F.; Cui, L.; Huang, P.; Yu, Y.; Wang, Y. *ACS Nano* **2010**, *4*, 681−688.